A Peak Detection Based OOK Photoacoustic Modulation Scheme for Air to Underwater Communication

Md Shafiqul Islam, Mohamed Younis, Muntasir Mahmud, Gary Carter, and Fow-Sen Choa
Department of Computer Science and Electrical Engineering
University of Maryland Baltimore County
Baltimore, Maryland, USA
mdislam1, younis, mmahmud1, carter, and choa@umbc.edu

***Abstract*—The popularity of underwater applications has been growing due to the major technological advances in the last few decades. Yet, direct communication from an airborne node to an underwater node remains challenging due to the inability of any known signal which propagates well in both the air and water mediums. Photoacoustic energy transfer is a promising mechanism for enabling such cross-medium communication. Although the use of the photoacoustic mechanism is quite common in medical imaging, little progress has been made on building the communication protocol stack. Most research studies have only focused on characterizing the channel and relating the laser and acoustic signals. Little attention has been given to developing suitable modulation and demodulation schemes. This paper fills such a technical gap and proposes a novel OOK modulation scheme using peak detection technique. We validate the effectiveness of our proposed scheme through simulation and lab experiments.**

***Keywords:* Photoacoustic communication; Underwater communication; Underwater optical networks; Modulation.**

I. INTRODUCTION

Communication technologies and increased connectivity have made major advances in recent years. Underwater environments are not an exception, where the viability of inter-node communication has attracted interest. Applications of underwater communication span many domains, namely, scientific, civil, and military. Examples of these applications include search-and-rescue, coastal patrol, oceanographic data collection, environmental monitoring, assisted navigation, and security surveillance, etc. Although radio frequency (RF) is the most popular spectrum to communicate in the air medium, it is not widely used for underwater communication due to its high attenuation coefficient in the water medium. On the other hand, an acoustic signal is the most popular choice for underwater communication because of its low attenuation coefficient in the water medium [1][2]. A typical architecture of an underwater network involves a set of nodes that are controlled or directed by an off-water command center.

Interfacing an underwater network with off-water command nodes is challenged by the lack of a proper cross-medium communication channel. There are no physical signals that work well in both air and water medium. Communication from air to underwater using acoustic signal is not a good choice because most of the energy of the acoustic signal is reflected back to the air from the air-water interface due to the high impedance mismatch between air and water [3]. RF signals also suffer high attenuation in the water, as noted earlier. Typically, underwater communication systems use floating nodes such as boats or buoys to act as a gateway. Such a gateway contains both radio and acoustic modems. A remote or airborne base-station establishes RF-based communication link with the gateway; upon receiving a message, the latter acts as a relay using an acoustic transceiver to pass the message to underwater receivers. However, the reliance on surface-based gateway nodes is undesirable in many applications for reasons ranging from logistical complications in deploying these nodes to security concerns where the gateway could be exploited to know where the underwater nodes are located. Therefore, interfacing the underwater network through an airborne base-station is desirable in many cases.

The use of visible light could be a viable option for cross-medium communication because of its high transmissivity from air to underwater medium [4]. In fact, the high bandwidth and low time latency make visible light more suitable for high-speed communication [5][6]. A bit rate of 400-Gb/s could be achieved using wavelength-division-multiplexing (WDM) and four-level pulse amplitude modulation (PAM4) for water-air-water link [6]. However, light propagation in the water medium is very limited because of its high attenuation coefficient in the water medium. Even for the purest water, the light can travel for a maximum of 200 meters [7][8]. Hence, visible light is good for scenarios where the distance between the airborne and underwater nodes is relatively short. For long range, the photoacoustic (PA) energy transfer mechanism is a promising method to communicate from an airborne node to an underwater node wirelessly. When high energy pulsed laser light impinges on a liquid medium like water, an acoustic signal is generated. Such a phenomenon is called the photoacoustic effect and can be categorized as linear and nonlinear; the latter generates a strong acoustic signal. PA is a viable option for long-range air-to-water communication because although light energy is sent from the transmitter, this light energy is converted to acoustic energy in the water which can travel a long distance in the water medium [9].

Although the use of PA is quite common in medical imaging, its consideration for air-to-water communication is relatively new. Most published work in this area has concentrated on analyzing the quality of the generated acoustic signal. Little effort has been dedicated to developing a communication protocol stack for PA, particularly devising modulation/demodulation schemes. The design of a suitable

modulation/demodulation scheme for PA is quite challenging for several reasons. First, the generated acoustic signal in the nonlinear PA process is very broadband in nature which makes it difficult to pursue FSK and PSK. Second, the acoustic signal strength at the receiver is variable, which makes the use of certain kinds of modulation techniques such as QAM very difficult. Third, the PA process is hybrid in nature, meaning that the transmitter is sending one kind of energy which is light, while the receiver is receiving another kind of energy, specifically acoustic. Because of such hybrid nature, the modulation and demodulation scheme are not reciprocal.

In this paper, we address the aforementioned issues and devise a novel modulation and demodulation technique using the On-Off Keying (OOK) methodology that is based on peak detection of the received acoustic signal. The key advantages of peak detection based OOK modulation (PDOOK) are that it is not sensitive to the broadband nature of the received signal and facilitates synchronizing the transmitter and receiver. These advantages simplify the transmitter and receiver design and also yield low bit error rate. In summary, the contributions of this paper are: (1) analyze the generated acoustic signal quality based on the laser light parameters and relative position of the transmitter and receiver, (2) propose and implement a novel modulation and demodulation scheme that provides the best results for hybrid communication system such as PA based on the above analysis, (3) show the performance of such a modulation and demodulation scheme in terms of the achievable bit rate and the bit error rate (BER), for different light parameters and varying receiver positions relative to the normal of the water surface at the laser light incident point, both by experiments and simulations.

The paper is organized as follows. The next section sets the contribution apart from related work in the literature. Section III provides some preliminaries and discusses the challenges of PA-based communication. Section IV describes PDOOK in detail and presents the transmitter and receiver design. The experiments and simulation results are reported in Section V. Finally, the paper is concluded in Section VI.

II. Related Work

Various methods have been explored to communicate from an airborne base-station to underwater nodes [5][10]. Visible light communication (VLC) has been pursued in multiple studies [4-8] [10-12]. Although VLC could achieve a high bit rate, the large attenuation coefficient of visible light makes VLC unfit for long-range communication. High energy laser light has been explored as well [13]. However, it is very difficult to focus laser light on a small receiver located underwater due to the water surface wave. Recently an MIT group has used translational acoustic-RF communication (TARF) for underwater to air unidirectional communication [14]. In TARF, an underwater acoustic source creates an acoustic signal which causes a displacement of the water surface when they impinge on the water-air boundary. This surface displacement can be detected by radar. TARF is effective for underwater-to-air communication, but it cannot be implemented for air-to-underwater communication. Microwaves could be another viable option for cross-medium communication. In [15], microwave-induced thermos-acoustic communication has been proposed and implemented for air to underwater communication. But signal strength of the generated acoustic signal through this process is not as strong as generated using the PA method.

Exploiting PA for air to underwater communication is a very promising method, especially over long distances. PA technology is quite popular in medical imaging [16]-[18] and industrial applications [19]. However, its uses for air to underwater communication is relatively new. There are some notable research works. In [20], low-cost passive relays are deployed on the water surface to minimize the energy required for PA communication. However, the placement of these passive relays is logistically very complicated and requires preplanning, in fact, it could be risky in some application scenarios, e.g., during combat. A fully wireless link between air and water is highly desirable for such a scenario. Moreover, the use of relays is applicable for linear optoacoustic links which are generally limited in range. Blackmon et al. [9] [21-22] have conducted a rigorous time and frequency domain analysis of the generated acoustic signal. The analysis has pointed out the dependency of the acoustic signal on the position of the acoustic receiver with respect to the axis of the laser beam.

The generated acoustic signal is usually very broadband; yet certain frequency components contain the maximum energy which is referred to as peak frequency. The relationship between peak frequency and input laser power has been studied in [23]. It has been shown that with the increase of laser power, the peak frequency decreases. A broadband acoustic signal is usually unsuited for long-range underwater communication because the higher frequencies attenuate quickly while propagating in water. Hence, a narrowband signal with low frequencies is desired. Y. H. Berthelot [24] has shown how to create a narrowband acoustic signal by controlling the laser repetition rate. Yet, the analysis is done only for a flat-water surface. In our prior work [25], we have shown how to create a narrowband signal even in the presence of a wavy water surface. All the above works mainly focus on PA signal generation, propagation, directionality, range calculation, etc. To our best knowledge, little attention has been given to design suitable PA modulation and demodulation schemes. In this paper, we opt to fill such a technical gap.

III. System Model and Design Challenges

This section covers some background about the PA mechanism and highlights the challenges for designing suitable modulation and demodulation schemes.

A. Photoacoustic Mechanism

Alexander Graham Bell first discovered the photoacoustic effect in 1881. He noticed that when high-intensity light impinges on a liquid like water, an acoustic signal is generated, a phenomenon that is referred to as the photoacoustic effect. Figure 1 describes possible cross-medium communication by exploiting photoacoustic energy conversion. The photoacoustic energy conversion process could be divided into two

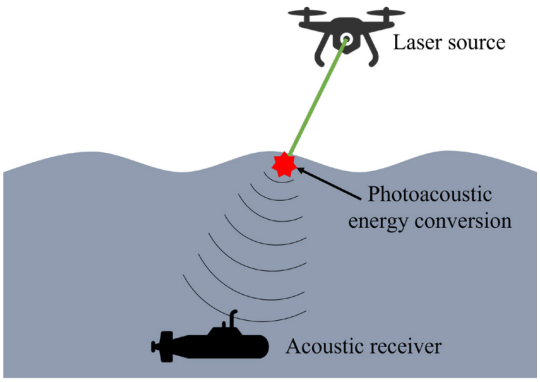

Fig. 1. Air to underwater communication using photoacoustic mechanism

mechanisms, linear and nonlinear. In a linear mechanism, high-intensity pulsed laser light is absorbed by the water and causes to water to heat up. Since the laser light is pulsed, a water temperature fluctuation occurs where laser light gets absorbed by the water. This temperature fluctuation introduces a change in density which eventually creates a region of compression and rarefaction. Such compression and rarefaction of the water generate a propagating pressure wave. This process is also known as thermo-acoustic. In this process, the properties of the water medium do not change. The term "linear" is associated because the intensity of the generated sound wave is proportional to the applied intensity of the laser light. The conversion rate in this process is very low which makes it inefficient for long distance communication [9][22].

This paper considers a nonlinear photoacoustic mechanism. In contrast to linear PA, in a nonlinear PA the generated acoustic signal strength is not proportional to the applied light energy, and the physical properties of the water medium change. When the intensity of the applied pulsed laser light energy exceeds a threshold level, the water becomes vapor and optical breakdown occurs. In this process water goes to a plasma state which creates optical breakdown induced acoustic shock waves. A nonlinear photoacoustic effect also creates additional cavitation bubble oscillation, which creates shockwaves as well. The energy conversion rate in a nonlinear optoacoustic process is much higher than the linear counterpart. It is reported on [22] that for a typical single pulse laser source the generated sound pressure level (SPL) is below 150 dB re μPa (decibel relative to a micro Pascal) at a meter distance for linear photoacoustic whereas the SPL is higher than 178 dB re μPa for nonlinear photoacoustic. The breakdown threshold depends on the duration of the laser pulse. A. Vogel et al. [16] have studied the required breakdown irradiance threshold for nanosecond and femtosecond lasers. It has been concluded that irradiance energy levels in the order of 10^{11} W/cm^2 and 10^{13} W/cm^2, are required for a nanosecond and a femtosecond laser, respectively. In order to create such high irradiance in the water we need to focus the laser light on the water. Hence, we have used focusing lenses in our lab experiments. The duration (τ), energy (E), diameter (D) of the laser beam and focal length (f)

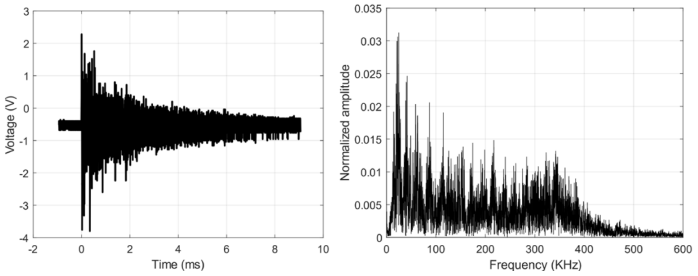

(a) (b)

Fig. 2. (a) Generated acoustic signal from a single laser pulse and (b) FFT of that acoustic signal

of the lens affect the value of laser irradiance in the water [26]. We can calculate the laser irradiance as follows,

$$I = \frac{\frac{E}{\tau}}{A_f} \tag{1}$$

where, A_f is the focal spot area which further can be calculated as follows,

$$A_f = \pi r^2 = \pi\left(\frac{\lambda f M^2}{\pi\frac{D}{2}}\right)^2 \tag{2}$$

where, λ is the wavelength of the laser light and M^2 is the beam quality factor of the laser beam. For a perfect Gaussian beam, the value of M^2 is 1. Hence, for a perfect Gaussian laser beam substituting the value of A_f from eq. (2) into eq. (1) we get,

$$I = \frac{\pi E}{4\tau}\left(\frac{D}{\lambda f}\right)^2 \tag{3}$$

We will use this equation to calculate the laser irradiance value in our lab experiments.

B. Design Challenges

There are four key issues that we must consider when designing a suitable modulation and demodulation scheme for PA-based communications. First, the generated acoustic signal using the PA effect is very broadband in nature. Figure 2 shows both the time (Figure 2a) and frequency (Figure 2b) domain plots of the generated acoustic signal for a single laser pulse using a nonlinear PA mechanism. From Figure 2b we can observe the generated acoustic signal has spectral response up to 500 KHz. Although by applying a pass band filter we can detect a narrowband signal, the signal will become very weak. Hence, pursuing a FSK type modulation is quite challenging for this kind of PA signal.

Second, in nonlinear PA the optical breakdown of the water creates a vapor cloud around the plasma position [22]. This vapor cloud blocks the subsequent acoustic signal generation. To avoid such a scenario, we must wait a reasonable amount of time before sending the next laser pulse which constrains the repetition rate of laser pulses and eventually limits the channel capacity. In [22], it has been experimentally shown that even at a laser pulse repetition rate of 200 Hz, there are several missing acoustic signals. Thirdly, even for fixed laser parameters the intensity of the generated acoustic signal could be inconsistent. This may be caused by imperfection in the laser source where

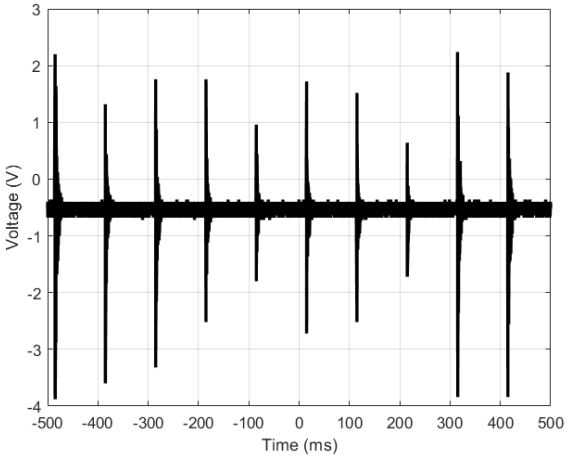

Fig. 3. Generated acoustic signal from a Q-switch Nd:Yag laser with repetition rate = 10 Hz

the generated laser pulses do not have the same power. We have observed such power variability in our experiments, while using a custom-made laser by NASA Goddard Space Flight Center. Figure 3 shows an experimental result of the generated acoustic signal where the repetition rate of the laser pulse is 10 *Hz*. From this figure we can see, the peak value of each generated acoustic signal is not the same. This kind of amplitude fluctuation and others, for example environmental conditions such as water waves, making any kind of PAM, and QAM, modulation schemes quite challenging.

The fourth issue is related to the hybrid nature of the carriers, where the PA effect involves two different types of signals. In a PA-based communication, light energy is emitted from the transmitter and acoustic energy is sensed at the receiver. Such hybrid nature complicates the design of a suitable modulation and demodulation scheme. Considering all the above design challenges, we believe that OOK is the simplest, yet effective modulation and demodulation scheme for the PA mechanism. In the next section, we will describe the transmitter and receiver design based on the OOK modulation scheme.

IV. Transmitter and Receiver Design

To design a suitable modulation scheme, we have studied the generated acoustic signal carefully. Figure 2a shows the pattern of the generated acoustic signal for a single pulse of the laser light. From this figure we can observe that for a single laser pulse generated acoustic signal has multiple peaks. The highest peak appears almost at the very beginning. Then the strength of the acoustic signal diminishes within a couple of milliseconds. Hence, we adopted a peak detection based OOK modulation (PDOOK) scheme, meaning that sending a bit value of '1' corresponds to emitting a laser pulse and for a value of '0' no pulse is triggered. Figure 4 shows the PDOOK modulated acoustic signal for a random data pattern '1011'. In order to demodulate this acoustic signal, a peak detector is to be employed to identify the first peak of the received acoustic signal and use such peak value as baseline for the rest of the bit transmission time, *T*. If the first peak continues to be the largest,

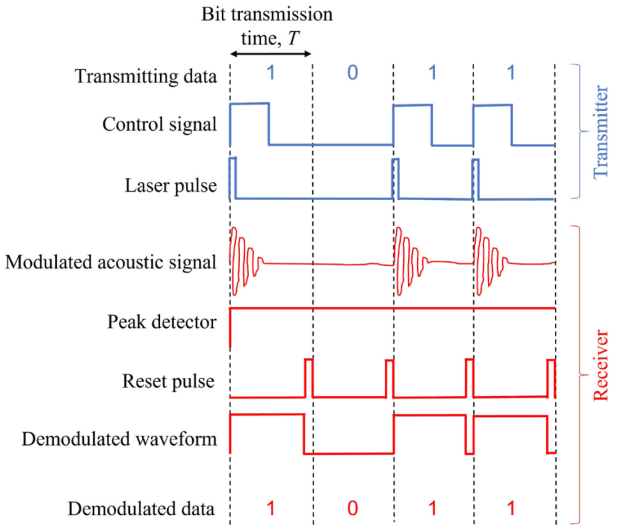

Fig. 4. Timing diagram of PDOOK signals

a bit value of "1" is concluded. However, the peak will be reset before the next bit transmission time. In order to do that we use an electric reset pulse to reset that peak level. Here we must keep in mind that bit transmission time, *T*, and laser pulse duration, τ are different, whereas τ is the duration of laser pulse whereas *T* is the laser pulse repetition time. In the balance of this section, we describe the design of the transmitter and receiver for our PDOOK modulation/demodulation.

A. *Transmitter Design*

Figure 4 shows the timing diagram for the signals required to implement our proposed PDOOK. Based on such a timing diagram, Figure 5 shows a complete block diagram of the PDOOK transmitter and receiver. The main objective of the PDOOK transmitter is to produce a laser pulse of specific energy and repetition rate based on the data to be sent and the achievable bit rate. The controller generates a random return to zero (*RZ*) type data sequence that drives the components which triggers the pulse generation in the laser. First, based on the input data, the controller creates a signal to produce the desired laser pulse. We choose a *RZ* type control signal since it helps to distinguish between consecutive '1's. The laser driver has three main components: oscillator, preamplifier, and amplifier. Based on the electronic signals, these three components enable producing laser pulses with a desired pulse duration, pulse repetition rate and laser pulse energy. In order to implement a nonlinear PA mechanism, a very powerful pulsed laser source is required. Usually a Q switch Nd:Yag laser can produce such a high energy nano or pico-second laser pulses.

B. *Receiver Design*

Figure 4 shows timing diagram for all the associated signals with a PDOOK receiver and Figure 5 provides a block diagram description of the receiver circuit. Functionally, we can divide the PDOOK receiver into the following:

Detection and amplification: At first, a hydrophone detects the PDOOK modulated acoustic signal. Since the modulated

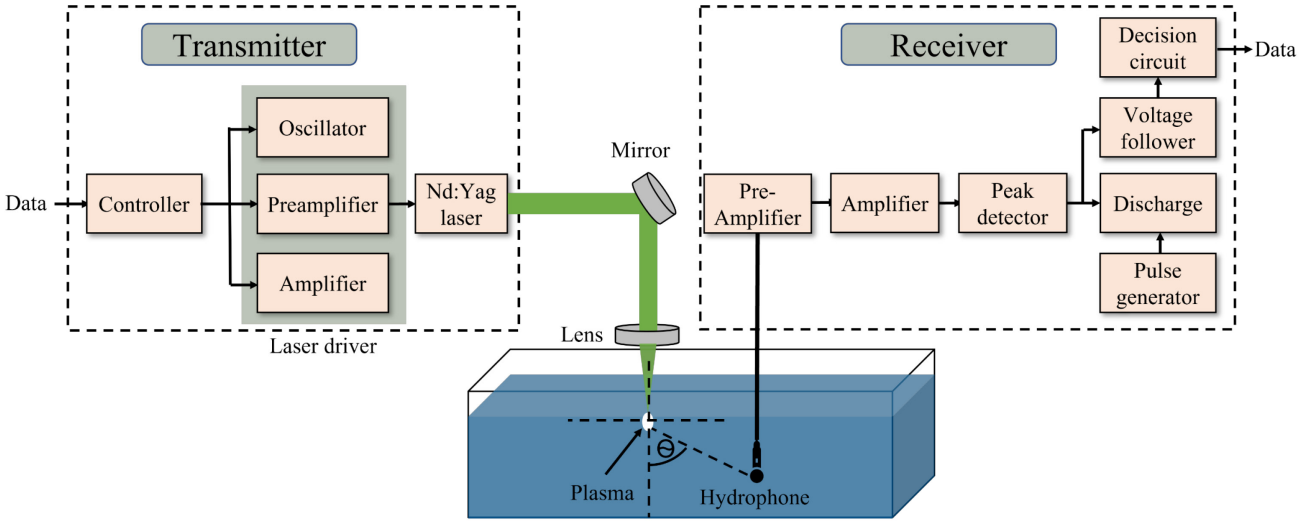

Fig. 5. Block diagram of the photoacoustic air-to-underwater communication

acoustic signal is very broadband, a hydrophone with a broad range of frequency response is required for this kind of receiver. Usually, an acoustic signal generated using a nonlinear PA mechanism can contain frequency components even in the MHz range. Though a higher frequency component mostly attenuates with the increase of the distance that the signal travels in the water, a hydrophone should sense at least a couple of hundreds KHz frequency components of the acoustic signal in order to successfully detect the signal at the receiver end. A pre-amplifier followed by an amplifier is used to produce a larger electrical signal.

Peak detector: After amplifying the signal, a peak detector is used to detect the maximum voltage of the acoustic signal. At the circuit level, a peak detector is realized using a capacitor. As shown in Figure 4, the detected signal peak should be latched for at least *T* sec, which can be achieved by choosing appropriate RC time constant. In order to successfully detect the next acoustic pulse (next transmitted bit), we need to reset (set to 0 V) the peak value at the beginning of every time period *T*. This could be done by using a small rectangular reset pulse at the end of every time period, *T*. The pulse generator block in Figure 5 is responsible for doing so. Such pulse generation requires time synchronization between the sender and receiver. Therefore, PDOOK requires that the first transmitted bit to logic '1', which constitutes a necessary overhead. In our receiver design, the detection of the first acoustic signal peak triggers the generation of a reset pulse.

Shaping: From Figure 3 we can see the peak intensity of every acoustic signal is not the same. Hence, we need a decision circuit to make all the peaks in the same level. Usually, a comparator is used as a decision circuit. We need to keep in mind that this decision circuit might change the overall circuit gain. A voltage follower circuit is required to maintain the desired voltage and current level of the receiver circuit. Figure 4 shows what a demodulated PDOOK signal looks like. Figure 6 shows an example of a receiver circuit that has been used for our experiment. The amplifier, voltage follower and comparator (decision circuit) all have been designed using op-amps. The amplifier is a non-inverting type whose gain can be controlled by the *R1* and *R2* resistors. The peak detector is composed of a diode, capacitor and two resistors *R3* and *R4*. The resistor *R3* has very high value and *R4* has very low value. A *BJT* switch has been used to switch between *R3* and *R4*. This switch is controlled by a reset pulse, which we discussed earlier. When the value of that reset pulse is *0* V, the peak detector is connected to the large resistor *R3* so that the *RC* time constant of the peak detector becomes higher. The higher *RC* time constant helps the receiver retain the peak value for a long period of time. When we need to reset the peak value at the end of every time period, *T*, a small reset pulse in the *BJT* base connects the peak detector with the lower resistor *R4*, so that the capacitor of the peak detector can discharge quickly. Finally, a comparator circuit in conjunction with a voltage follower produces the two fixed voltage levels to successfully distinguish between logic '*1*' and '*0*'.

V. Validation Results

Both lab experiments and simulations have been conducted to validate our proposed PDOOK transmitter and receiver design. In this section, we will start discussing the lab experiments and then present simulation results which further capture the performance of PDOOK in a noisy environment.

A. Lab Experiments

Experiment Setup: In our experiments, the Geoscience Laser Altimeter System (GLAS) Q-switch Nd:Yag laser has been used as a light source [27]. The pulse duration of this laser source is 6 ns with energy of 1 ~ 50 mj per pulse. The diameter of the laser beam is 2 cm. It can produce a maximum of 40 Hz repetition rate. In order to control the laser driver and create control signals, a delay generator (DG535) has been used [28]. A Xilinx FPGA (Artix-7) has been used to generate random patterns of pulse periods and control the output of a delay generator [29]. Mirror and focusing lenses have been used to focus the laser light on the water and produce different laser

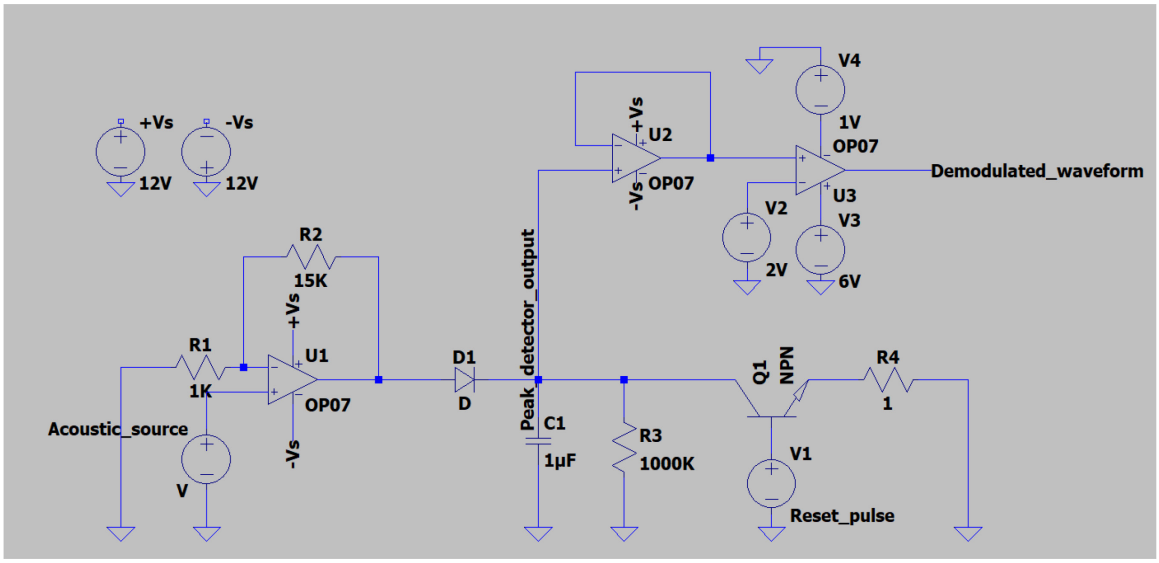

Fig. 6. Schematic diagram of the acoustic receiver circuit

irradiance in the water. In our experiments, we have used lenses of 20 cm and 7.5 cm focal lengths. We have used laser pulse energies ranging from 20 mj to 50 mj. For example, if we choose 20 mj laser pulse energy and 20 cm focusing lens, by using eq. (3) we can produce 5.8×10^{11} $\mathrm{Wcm^{-2}}$ irradiance in the water which is above the breakdown threshold irradiance mentioned in Section III.

A 1.27m (L) x 0.6m (W) x 0.8m (H) water tank was used in the experiments. The tank is made of clear glass. Sound absorbing material is placed on the inner sides and bottom of the tank to mitigate reflection of acoustic signals. Given the constrained tank size, we placed our hydrophone at a maximum distance of 30 cm from the laser pulse focusing point. The hydrophone was placed at two different positions, namely, $\theta = 90^{\circ}$ and $\theta = 0^{\circ}$, from the vertical axis (norm on the water surface) of the laser light focusing point. Since the generated acoustic signal is very broadband, we have used the TC4014 hydrophone [30], which can detect acoustic signals up to 480 KHz. Such a hydrophone has a receiving sensitivity of -186dB ±3dB re 1V/µPa. The hydrophone is connected with an active input module (EC6076) which provides power to the hydrophone [31]. Figure 7 shows our experimental setup.

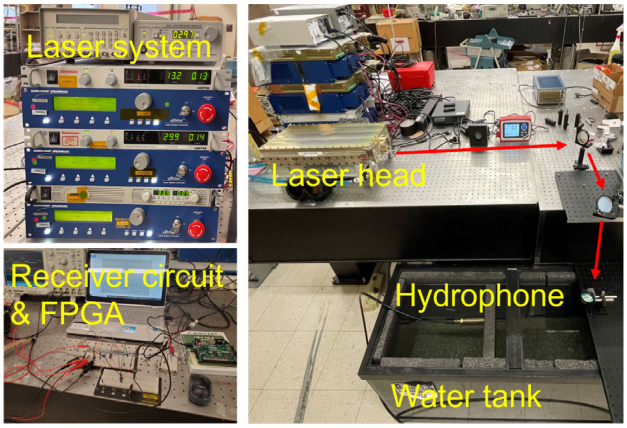

Fig. 7. Depicting the experimental setup for air-to-underwater PA communication

Experimental Results: To validate our modulator/demodulator design, at first, we transmitted a random bit pattern '110110011' at a repetition rate 10 Hz. Figure 8 shows the corresponding signals at the different stages of modulation/demodulation, as captured by a Tektronix DPO4054 digital oscilloscope. The topmost signal in the figure is the control signal based on the above bit pattern which is used to generate a sequence of laser pulses. The next signal is the modulated acoustic signal that reaches the receiver. Then, we show the PDOOK demodulated waveform before and after passing the decision circuit.

To further assess the design robustness, we have varied the laser pulse energy and observed the signal strength of the demodulated acoustic signal for various laser pulse repetition rates. The results are shown in Figure 9. We have used 20 cm and 7.5 cm lenses to focus the laser light inside the water. Figure 9a shows the signal strength for a laser repetition rate

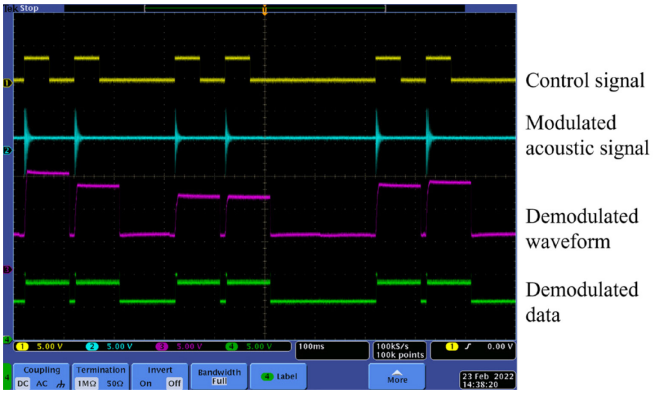

Fig. 8. Tx and Rx data for laser pulse energy 30 mj and repetition rate 10 Hz

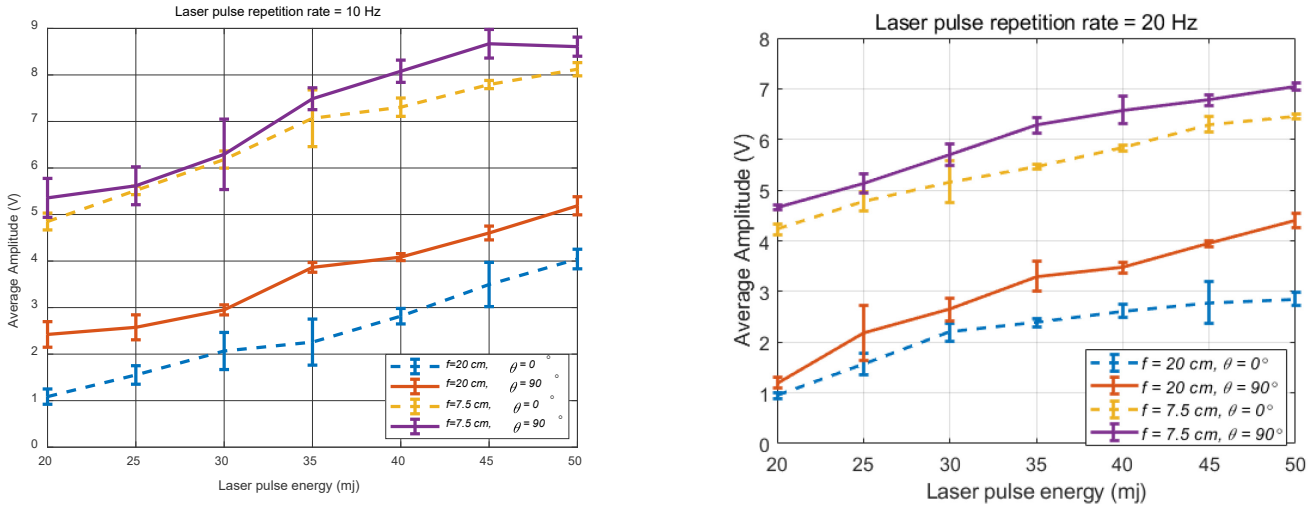

(a) **(b)**

Fig. 9. Effect of laser pulse energy on the received acoustic signal strength for laser repetition rate (a) 10 Hz and (b) 20 Hz

10 Hz. As expected, the increase of laser pulse energy boosts the strength of the received acoustic signals. There are two additional important notes to make about the results. First, the 7.5 cm focusing lens yields a stronger signal than the 20 cm lens, which is attributed to the creation of more irradiance, as indicated by eq. (3). Second, the received acoustic signal is directional, where a stronger signal is received when the hydrophone is placed at $\theta = 90^{\circ}$ than at $\theta = 0^{\circ}$. This observation is consistent with some experimental results found in the literature, e.g., in [23]. This kind of directivity depends on the generated plasma shape. Plasma could have different shapes, for example spherical or cylindrical. In our case the plasma is cylindrically shaped, and hence the signal strength is higher in one direction than the other.

The effect of focusing lenses is more significant than the hydrophone position. Figure 9b shows the results for a higher laser pulse repetition rate, specifically 20 Hz. The obtained results resemble those in Figure 9a, yet in all cases the received signal strength is a bit smaller than for a 10 Hz repetition rate. This is mainly because a higher repetition rate grows the probability of creating a vapor cloud which blocks subsequent pulses, as mentioned earlier in section III [22]. The effect of vapor cloud could be mitigated by using beam steering techniques. Employing a modulation technique which requires sending a smaller number of acoustic pulses could also reduce the effect of vapor cloud. In our future work, we will focus on how to diminish the impact of the vapor cloud on PA communication.

We further show the effect of laser pulse repetition rate on received signal strength in Figure 10. As expected, with the increase of laser repetition rate, the received signal becomes weaker. Figure 10a and 10b show the result for laser pulse

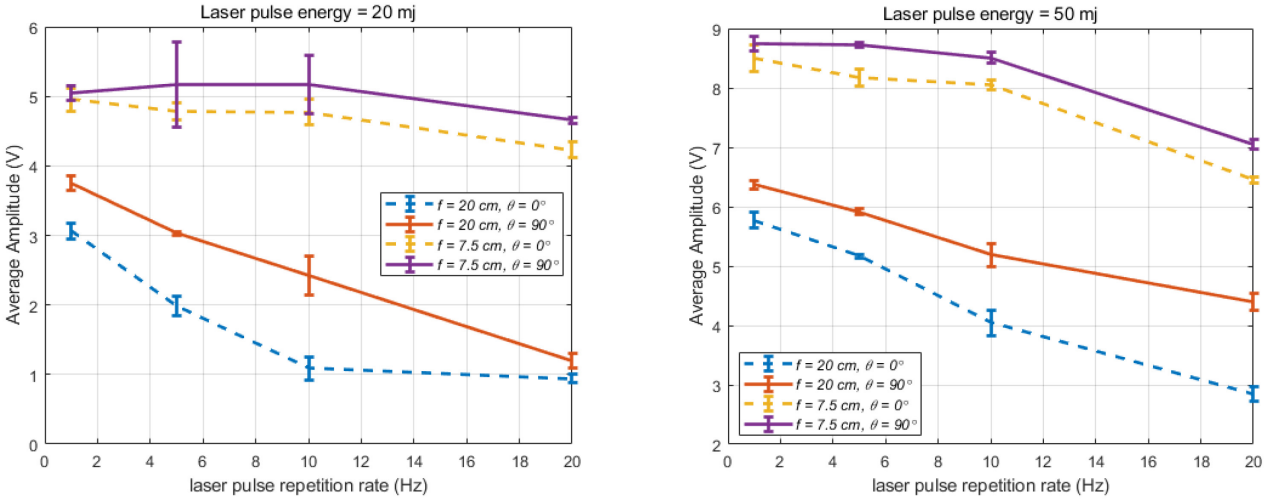

(a) **(b)**

Fig. 10. Effect of laser repetition rate on received acoustic signal strength for laser pulse energy (a) 20 mj and (b) 50 mj

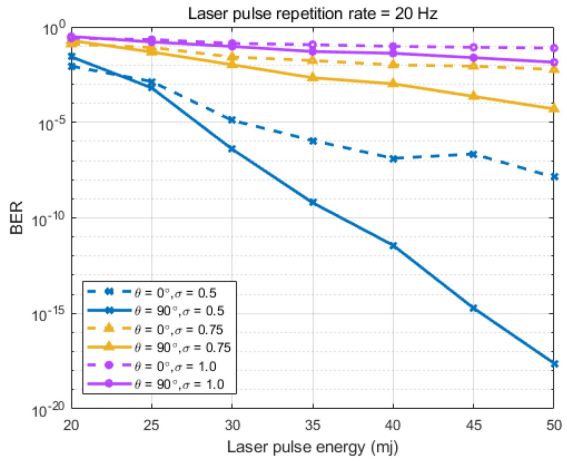

Fig. 11. *BER* vs laser pulse energy for laser repetition rate 20 Hz for different noise levels

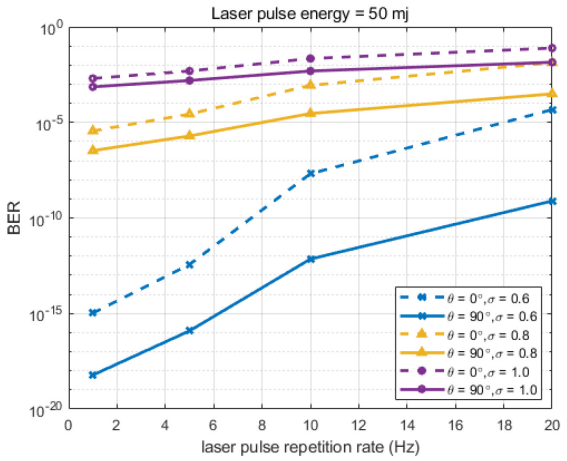

Fig. 12. *BER* vs laser pulse repetition rate laser pulse energy for pulse energy 50 mj for different noise levels

energy of 20 mj and 50 mj, respectively. Again, the a 7.5 cm focusing lens creates stronger acoustic signals than the 20 cm counterpart. We also observe that positioning the hydrophone at $\theta = 90^{\circ}$ provides a better signal than $\theta = 0^{\circ}$. Moreover, the variation in acoustic signal strength becomes smaller with the decrease of the laser repetition rate. This is mainly because the effect of vapor is more significant at high repetition rates.

B. Simulation Results

The aforementioned lab experiments have been conducted to show the performance of PDOOK at very short distance in a lab environment and in the presence of electrical noises only. Yet, in a real ocean environment, there could be other ambient noises that cannot be replicated in a lab prototype. Hence, we have pursued simulation to study the effect of ambient noises on the bit error rate (BER) and signal-to-noise ratio (SNR) performance of our proposed PDOOK modulation scheme.

BER calculation: At first, we injected random ambient noise and determined its effect on BER. We have assumed the ambient acoustic noise to be the additive white Gaussian noise (AWGN), and consequently calculated the error probability using the Q-function [32]. The Q-function of the noisy signal can be defined as follows:

$$Q\left(\frac{t-\mu}{\sigma}\right) = \frac{1}{\sqrt{2\pi\sigma^2}} \int_t^{\infty} \frac{e^{-(x-\mu)^2}}{2\sigma^2} dx \qquad (4)$$

where, μ and σ^2 are the mean and the variance of the noise distribution, respectively. The above Q-function indicates the probability that a Gaussian random variable x will obtain a value larger than t. Our proposed modulation technique is OOK type modulation, which means it has two states: (i) logic '0' indicated by no (zero voltage) reception, and (ii) logic '1' implied by V_p voltage reception. Here, V_p is the voltage amplitude at a receiver which has been shown in Figure 9 and 10. For varying laser pulse energy and repetition rate, respectively. If the threshold voltage for distinguishing between these two stages is $\frac{V_p}{2}$, based on eq. (4), the probability of erroneously detecting a logic stage can be defined as,

$$P(err) = BER = \frac{1}{\sqrt{2\pi\sigma^2}} \int_{\frac{V_p}{2}}^{\infty} \frac{e^{-(x)^2}}{2\sigma^2} dx \qquad (5)$$

Here we assume the mean of the noise is 0. Now combining eq. (4) and eq. (5), we can conclude,

$$BER = Q\left(\frac{V_p}{2\sigma}\right) \qquad (6)$$

Figure 11 shows the value of *BER* for different noise levels, σ and is plotted based on eq. (4)-(6). The simulation is done using MATLAB and based on a laser repetition rate of 20 Hz. We can observe from the figure that with the increase of σ (the noise), the value of *BER* increases which is expected. The results have been shown for a receiver positioned at 0° and 90°, where the value of *BER* is higher for 0° position [33]. Intuitively, when the received signal is stronger the value of *BER* is low; by considering Figure 9b and Figure 10 collectively give us an idea how much laser pulse energy is required in order to fulfill a certain *BER* requirement in a communication channel based on the noise level.

Similarly, Figure 12 shows the effect of the laser pulse repetition rate on the *BER* calculation for various noise levels. The simulation is performed for a fixed laser pulse energy of 50 mj. Here, we observe that with the increase of the laser pulse repetition rate, the *BER* grows which is also expected, because from Figure 10b we observe that with the increase of laser pulse repetition rate, the received signal strength diminishes. Figures 10b and 12 point out the value of maximum laser pulse repetition rate, i.e., what maximum bit rate is required for maintaining a certain *BER* value based on the noise level.

SNR calculation: Next, we determine the effect of noise on SNR for various underwater depths. In the lab experiments, we have measured sound pressure level (SPL) at relatively close proximity from the generated plasma (acoustic source). In order to determine SPL at a further depth (longer distance), we need to factor the acoustic path loss model and ambient acoustic noise at that depth. Acoustic path loss (PL) can be estimated in dB as follows [34]:

$$PL(f) = k \cdot 10 \log D + D \cdot 10 \log a(f) \qquad (7)$$

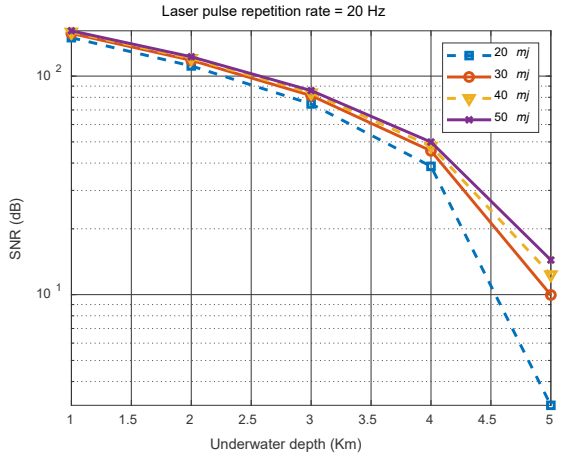

Fig. 13. *SNR* vs underwater depth for different laser pulse energy

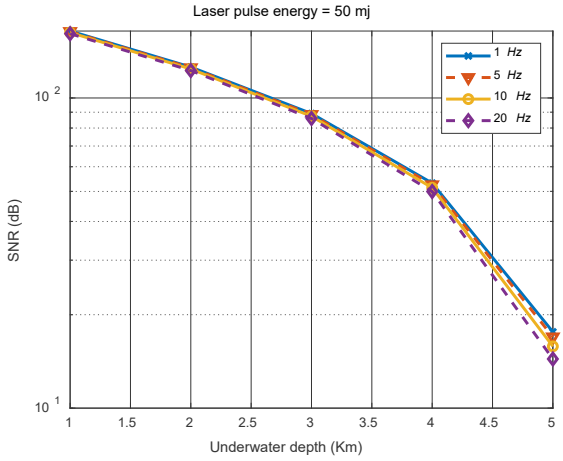

Fig. 14. *SNR* vs underwater depth for different laser pulse repetition rate

where, D is the underwater distance in km, k is the spreading factor, f is the acoustic source frequency in KHz, and a is the absorption coefficient. The spreading factor, k, determines the geometric shape of the acoustic propagation path; the value of k is 1.5 for so-called practical spreading [34]. The absorption coefficient, a, can be determined using Thorp's formula as follows [35]:

$$10\log a(f) = 0.11\frac{f^2}{1+f^2} + 44\frac{f^2}{4100+f^2} + 2.75\times 10^{-4}f^2 + 0.003 \quad (8)$$

The acoustic noise in an underwater environment has been modeled in [34], where turbulence, shipping, waves, and thermal noises are the main contributors. The power spectral density of these noise sources can be described by following empirical equations:

$$10\log N_t(f) = 17 - 30\log f \quad (9)$$

$$10\log N_s(f) = 40 + 20(s-0.5) + 26\log f - 60\log(f+0.03) \quad (10)$$

$$10\log N_w(f) = 50 + 7.5w^{\frac{1}{2}} + 20\log f - 40\log(f+0.4) \quad (11)$$

$$10\log N_{th}(f) = -15 + 20\log f \quad (12)$$

Thus, the total noise $N(f)$ can be expressed as:

$$10\log N(f) = 10\log N_t(f) + 10\log N_s(f) + 10\log N_w(f) + 10\log N_{th}(f) \quad (13)$$

In the above equations, s is the shipping activity factor whose value ranges from 0 to 1 and w is the wind speed in m/s. Using eq. (7) - (13), we can calculate the SNR in dB as follows:

$$SNR = SPL - PL - N \quad (14)$$

All the parameters in eq. (14) must be measured in dB.

Figure 13 shows the simulation results for SNR for various underwater depths. In this simulation, $w = 10$ m/s and $s = 1$. As expected, with the increase in the underwater depth, the SNR diminishes. The values of SNR have been shown for different settings of laser pulse energy at the transmitter side. With the increase of laser pulse energy, unsurprisingly the SNR also grows. Figure 14 shows the effect of laser pulse repetition rate on SNR for various underwater depths. We can observe from the figure that the SNR becomes slightly smaller at higher laser repetition rates especially at longer underwater depths. This is mainly because at higher laser pulse repetition rates, the acoustic signal is relatively weaker, as shown in Figure 10. Figure 13 and 14 point out the laser pulse energy and repletion rate required to obtain a certain amount of SNR for a known noisy channel.

VI. Conclusions

The photoacoustic effect can be an effective means for establishing communication across the air-water interface. However, the change of the carrier type from optical to acoustic makes the modulation/demodulation process quite complicated. This paper tackles such a challenge by first analyzing the properties of the generated acoustic signal based on the different laser parameters and relative positions of the transmitter and receiver. We have further investigated the key transmitter and receiver design issues and proposed a novel peak detection based OOK (PDOOK) modulation scheme. The paper has presented the design of the PDOOK transmitter and receiver and provided details for the various modules. We have validated our design through extensive experiments using a lab-based prototype. Based on the experimental results, creating strong acoustic signals underwater, one would need to focus laser light tightly inside the water and the relative position between transmitter and receiver needs to be 90°. The effect of ambient acoustic noises is further captured through simulation to provide guidelines for appropriate setting of the laser repetition rate and pulse energy.

Acknowledgment: This work is supported by the National Science Foundation, USA, Contract #0000010465. We want to express our gratitude to Dr. Anthony Yu from NASA Goddard Space Flight Center for enabling us to access the Geoscience Laser Altimeter System (GLAS) Q-switch Nd:Yag laser.

REFERENCES

[1] G. F. Edelmann, T. Akal, W. S. Hodgkiss, Seongil Kim, W. A. Kuperman and Hee Chun Song, "An initial demonstration of underwater acoustic communication using time reversal," *IEEE Journal of Oceanic Engineering*, 27(3), pp. 602-609, July 2002.

[2] S. Sendra, J. Lloret, J. M. Jimenez and L. Parra, "Underwater Acoustic Modems," *IEEE Sensors Journal*, 16(11), pp. 4063-4071, June 2016.

[3] O. A. Godin, "Transmission of Low-Frequency Sound through the Water-to-Air Interface," *Acoustic Physic*, vol. 53, no. 3, pp. 305–12, 2007.

[4] M. S. Islam and M. F. Younis, "Analyzing visible light communication through air–water interface," *IEEE Access*, vol.7, pp. 123830-123845, 2019.

[5] L. -K. Chen, Y. Shao and Y. Di, "Underwater and Water-Air Optical Wireless Communication," *Journal of Lightwave Technology*, vol. 40, no. 5, pp. 1440-1452, March 2022.

[6] H. H. Lu, et al., "A 400-Gb/s WDM-PAM4 OWC system through the free-space transmission with a water–air–water link," *Scientific Reports* Vol. 11, # 21431, 2021.

[7] Y. Dai, et al., "200-m/500-Mbps underwater wireless optical communication system utilizing a sparse nonlinear equalizer with a variable step size generalized orthogonal matching pursuit," *Opt. Express*, Vol. 29, pp. 32228-32243, 2021.

[8] M.V. Jamali, A. Chizari, and J. A. Salehi, "Performance Analysis of Multi-Hop Underwater Wireless Optical Communication Systems," *IEEE Photonics Technology Letters*, Vol. 29, pp. 462-465, Jan. 2017.

[9] F. Blackmon, L. Antonelli, "Remote, aerial, opto-acoustic communications and sonar," *Proc. SPIE 5778, Sensors, and Command, Control, Communications, and Intelligence (C3I) Technologies for Homeland Security and Homeland Defense IV*, May 2005.

[10] H. Luo, J. Wang, F. Bu, R. Ruby, K. Wu, and Z. Guo, "Recent Progress of Air/Water Cross-Boundary Communications for Underwater Sensor Networks: A Review," *IEEE Sensors Journal*, vol. 22, no. 9, pp. 8360-8382, 1 May1, 2022.

[11] X. Sun et al., "Field Demonstrations of Wide-Beam Optical Communications Through Water–Air Interface," *IEEE Access*, vol. 8, pp. 160480-160489, 2020.

[12] T. Lin, C. Gong, J. Luo, and Z. Xu, "Dynamic Optical Wireless Communication Channel Characterization Through Air-Water Interface," *Proc. of the IEEE/CIC International Conference on Communications*, China, 2020, pp. 173-178.

[13] C. J. Carver, et al., "AmphiLight: Direct Air-Water Communication with Laser Light," Proc. *USENIX Symposium on Networked Systems Design and Implementation (NSDI)*, 2020.

[14] F. Tonolini and F. Adib, "In Networking across Boundaries:Enabling Wireless Communication through the Water-Air Interface," *Proc. of the Conf. ACM Special Interest Group on Data Commun.*, 2018, pp. 117–31.

[15] X. Wang et al., "Microwave-Induced Thermoacoustic Communications," *IEEE Trans. Microwave Theory Tech.*, vol. 65, no. 9, 2017, pp. 3369–78.

[16] A. Vogel, J. Noack, G. Hüttman, et al. Mechanisms of femtosecond laser nanosurgery of cells and tissues. *Appl. Phys. B 81*, 1015–1047, 2005.

[17] A. Vogel, S. Busch, and U. Parlitz, "Shock wave emission and cavitation bubble generation by picosecond and nanosecond optical breakdown in water," *J. Acoust. Soc. Am.,* 100, pp. 148-165, 1996.

[18] A. De La Zerda et al., "Carbon Nanotubes as Photoacoustic Molecular Imaging Agents in Living Mice," *Nature Nanotech.*, vol. 3, no. 9, pp. 557–62, 2008.

[19] H. Chen, Y. Shi, and D. Xing, "Photoacoustic Thermorelaxation Microscopy for Thermal Diffusivity Measurement," *Opt. Lett.*, vol. 44, no. 13, pp. 3366–69, 2019.

[20] Z. Ji, Y. Fu, J. Li, Z. Zhao and W. Mai, "Photoacoustic Communication from the Air to Underwater Based on Low-Cost Passive Relays," *IEEE Communications Magazine*, vol. 59, no. 1, pp. 140-143, January 2021.

[21] F. Blackmon, L. Estes, and G. Fain, "Linear optoacoustic underwater communication*," Appl. Opt.,* 44, pp. 3833-3845, 2005.

[22] F. Blackmon and L. Antonelli, "Experimental demonstration of multiple pulse nonlinear optoacoustic signal generation and control," *Appl. Opt. 44*, 103-112, 2005.

[23] T.G. Jones, M. Helle, A. Ting, and M. Nicholas, "Tailoring Underwater Laser Acoustic Pulses," *NRL REVIEW, acoustics*, pp. 142-143, 2012.

[24] Y. H. Berthelot, "Thermoacoustic generation of narrow-band signals with high repetition rate pulsed lasers," *J. Acoust. Soc. Am.*, 85, pp. 1173–1181, 1989.

[25] M. S. Islam, M. Younis and F. -S. Choa, "Optimizing Acoustic Signal Quality for Linear Optoacoustic Communication," *Proc. of the IEEE International Conference on Communications (ICC)*, 2021, pp. 1-6.

[26] M. Mahmud, M. S. Islam, M. Younis and G. Carter, "Optical Focusing-based Adaptive Modulation for Optoacoustic Communication," *Proc. 30th Wireless and Optical Comm. Conf. (WOCC)*, 2021, pp. 272-276.

[27] https://ntrs.nasa.gov/api/citations/20070017920/downloads/20070017920.pdf

[28] https://www.valuetronics.com/product/dg535-stanford-research-pulse-generatorused?gclid=Cj0KCQiA2sqOBhCGARIsAPuPK0gOIl__yWR8d5_0Ws3_iLy02vjT0xvEwisbktVl1b0Rh9c3qosQG50aAgsVEALw_wcB

[29] https://digilent.com/reference/programmable-logic/nexys-4-ddr/start

[30] http://www.teledynemarine.com/reson-tc-4014

[31] http://www.teledynemarine.com/RESON-EC6076

[32] http://web.mit.edu/6.02/www/currentsemester/handouts/L08_slides.pdf

[33] Y. Tagawa, S. Yamamoto, K. Hayasaka, & M. Kameda, "On pressure impulse of a laser-induced underwater shock wave," *Journal of Fluid Mechanics*, vol. 808, pp. 5-18, 2016.

[34] M. Stojanovic, "On the relationship between capacity and distance in an underwater acoustic communication channel," *SIGMOBILE Mob. Comput. Commun. Rev.*, vol.11, issue 4, pp.34–43, October 2007.

[35] L. Berkhovskikh, and Y. Lysanov, "Fundamentals of Ocean Acoustics," New York: Springer, 1982.